communications biology

A Nature Portfolio journal

Article

https://doi.org/10.1038/s42003-025-08435-8

Exposure to COVID-19 virus-like particles modulates firing patterns of cortical neurons in the mouse brain

Aniruddha Das[1,6], Jacob Icardi[1,6], Julie Borovicka[1], Sarah Holden[2], Henry F. Harrison[3], Alec J. Hirsch[3], Jacob Raber[2,4] & Hod Dana[1,5]

Severe Acute Respiratory Syndrome Coronavirus 2 (SARS-CoV-2) causes a systemic infection that affects the central nervous system. However, its high infectivity makes comprehensive research with the active virus challenging. Here, we use virus-like particles (VLPs) to explore how exposure to SARS-CoV-2 proteins affects brain activity patterns in wild-type mice and in mice that express the human tau protein. VLP exposure elicits changes in corticosterone and distinct chemokine levels. Longitudinal two-photon microscopy recordings in primary somatosensory and motor cortices reveal substantial short-term increases in cortical activity in VLP-injected mice, with increased stimulus-evoked activity in both genotypes and elevated spontaneous activity in the human tau genotype only. Vehicle-injected human tau mice also show increases in cortical activity patterns. Over the following weeks, activity metrics partially subside but do not completely return to baseline levels. Overall, our data suggest that exposure to SARS-CoV-2 VLPs leads to strong short-term disruption of cortical activity patterns in mice with long-term residual effects. Middle-aged human tau mice, which have a more vulnerable genetic background and overexpression of the tau protein, exhibit more severe pathobiology and may be at risk for more adverse outcomes.

Infection by Severe Acute Respiratory Syndrome Corona Virus 2 (SARS-CoV-2) or one of its newer derivatives may cause systemic harm to the human body, including the brain. Reported brain-related pathologies include changes to synaptic homeostasis[1], fusion of neurons to neurons and/or glial cells that compromise neuronal firing[2], as well as reduced burst activity of neurons[3]. Such modified neuronal physiology may lead to behavioral alterations and cognitive deficits, which may be of major concern due to the wide spread of the virus. Moreover, at-risk populations due to age, health condition, and/or genetic risk factors of age-related cognitive decline and neurodegenerative disorders, such as in the elderly or patients with Alzheimer's disease (AD), may suffer more from COVID-19 complications or long-term effects than the general population[4–6].

The infectious nature of SARS-CoV-2 makes comprehensive studies with it challenging, which has led to a search for appropriate models that would allow conducting experiments in a safer environment. Such an alternative model is using virus-like particles (VLPs), which express the SARS-CoV-2 essential proteins without the replicating viral RNA[7–9]. The SARS-CoV-2 VLPs allow studying their effects on the host organism without the associated risk of being exposed to the virus itself. Previous works with VLPs showed their usefulness for testing how different SARS-CoV-2 mutations like Delta and Omicron affected virus infectivity in the presence of vaccines[10], or to study the role of different protein mutations on virus infectivity[11].

Exposure to the SARS-CoV-2 virus, or to its VLPs, is expected to cause a systemic immune response with multiple potential outcomes, including activation of glial cells in the central nervous system and initiation of inflammatory responses. Therefore, such exposure would also affect neurons in the brain and may modulate their activity patterns[12–14]. The immune response is expected to decrease over time, but it remains unclear whether there would be long-term changes in brain functionality. Moreover, such effects may be further amplified by existing health conditions, which may relate to genetic factors and/or age, and would make the patient or an animal

[1]Department of Neurosciences, Lerner Research Institute, Cleveland Clinic Foundation, Cleveland, OH, USA. [2]Department of Behavioral Neuroscience, Oregon Health & Science University, Portland, OR, USA. [3]Vaccine and Gene Therapy Institute, Oregon Health & Science University, Beaverton, OR, USA. [4]Departments of Neurology and Radiation Medicine, Division of Neuroscience, ONPRC, Oregon Health & Science University, Portland, OR, USA. [5]Department of Molecular Medicine, Cleveland Clinic Lerner College of Medicine, School of Medicine, Case Western Reserve University, Cleveland, OH, USA. [6]These authors contributed equally: Aniruddha Das, Jacob Icardi. e-mail: danah@ccf.org

model more vulnerable to viral exposure. Therefore, proper assessment of the exposure effect on the brain may benefit from the use of longitudinal methods, which will allow for studying the progression of pathology within the same subject over time.

Here, we conducted repeated recordings of neuronal activity in mice 11–13 months old before and after exposure to SARS-CoV-2 VLPs. We compared the activity patterns between C57BL6/J wild-type mice and C57BL6/J mice that express the human tau protein at an age range where they exhibit substantial tau-related pathologies[15–18]. The involvement of tau is particularly interesting since the SARS-CoV-2 virus exposure was reported to trigger tau pathology[19–22], and the expression of tau may affect neuronal functionality[23]. In addition, tau pathology is more common in AD patients, who are at increased risk of complications related to COVID-19[24]. Mice were first injected with VLPs to assess the dose-dependent response of their immune systems. Then, we recorded spontaneous and stimulated activity patterns from cortical neurons in the motor and somatosensory cortices using two-photon laser scanning microscopy (TPLSM)[25] before and after exposure to a selected dose of VLPs. Our findings show strong short-term effects of exposure to VLPs on brain activity metrics, with residual long-term effects and increased vulnerability in htau mice.

Results

Finding the optimal VLP dose to achieve a robust immune response

VLPs were generated, similar to our previous report[9], to express the SARS-CoV-2 nucleocapsid (N), membrane (M), and envelope (E) structural proteins together with the spike protein (S), allowing us to perform SARS-CoV-2-related studies without replicating virus and outside of a BSL-3 facility. Mice were injected ($n = 19$ mice; intraperitoneal (IP)) with different doses of VLPs or vehicle solutions. One hour later, blood samples were collected and the levels of Chemokine (C-C motif) ligand 7 (CCL7) and corticosterone hormone in the plasma were analyzed to assess activation of the immune system by exposure to the VLPs. VLP injection, at 0.3 μg or 1 μg per mouse, significantly reduced plasma levels of CCL7 with a similar effect seen at both dosages (Fig. 1A). In addition, the injection of 1 μg VLPs significantly increased corticosterone levels 1 h after VLP injection, while 0.3 μg VLPs showed no significant change compared to vehicle injection (Fig. 1B).

As the hippocampus plays an important role in regulation of the hypothalamic-pituitary-adrenal axis and the regulation of plasma corticosterone levels[9,26,27], twenty-four hours after the VLP injection, all mice were euthanized, and hippocampal tissue was extracted and processed. The concentrations of three chemokines that indicate activation of the immune system showed a U-shape pattern with positive correlations between the measured proteins. The concentration of Chemokine (C-C motif) ligand 3 (CCL3) was decreased following injection of 0.3 and slightly decreased with injection of 1 μg VLPs. We found a similar pattern with the concentration of Intercellular Adhesion Molecule 1 (ICAM-1, also known as Cluster of Differentiation 54, CD54), which plays an important role in mediating immune and inflammatory responses and is known for regulating leukocyte recruitment from circulation to sites of inflammation[28]. Finally, the concentration of the murine LPS-induced CXC chemokine (LIX), which is a neutrophil-chemoattractant CXC chemokine and is involved in recruitment of neutrophils to sites of inflammation[29], was also decreased following injection of 0.3 and slightly decreased upon the injection of 1 μg of VLPs (Fig. 1C–E). Notably, there was a positive correlation between hippocampal levels of ICAM-1 and CCL3, LIX and CCL3, and ICAM-1 and LIX (Fig. 1F–H; $r = 0.71$, 0.83, and 0.82, respectively; Pearson's correlation). Based upon these findings, the 0.3 μg dose was selected for the cortical activity recording experiments described below, as it caused a similar reduction in plasma CCL7 levels as the 1 μg dose without the increase in corticosterone levels (Fig. 1A).

Monitoring baseline cortical activity revealed differences between WT and htau mice

jGCaMP7s was expressed in neurons within two sub-regions of the mouse primary somatosensory cortex corresponding to the hindlimb area ($S1_{HL}$) and the barrel field ($S1_{BF}$), as well as in two sub-regions of the primary motor cortex corresponding to the limbs ($M1_{limbs}$) and vibrissa and neck ($M1_{VN}$), as defined by mouse atlas coordinates[30]. Spontaneous activity of layer II/III neurons was recorded from all these four sub-regions. The responses of the

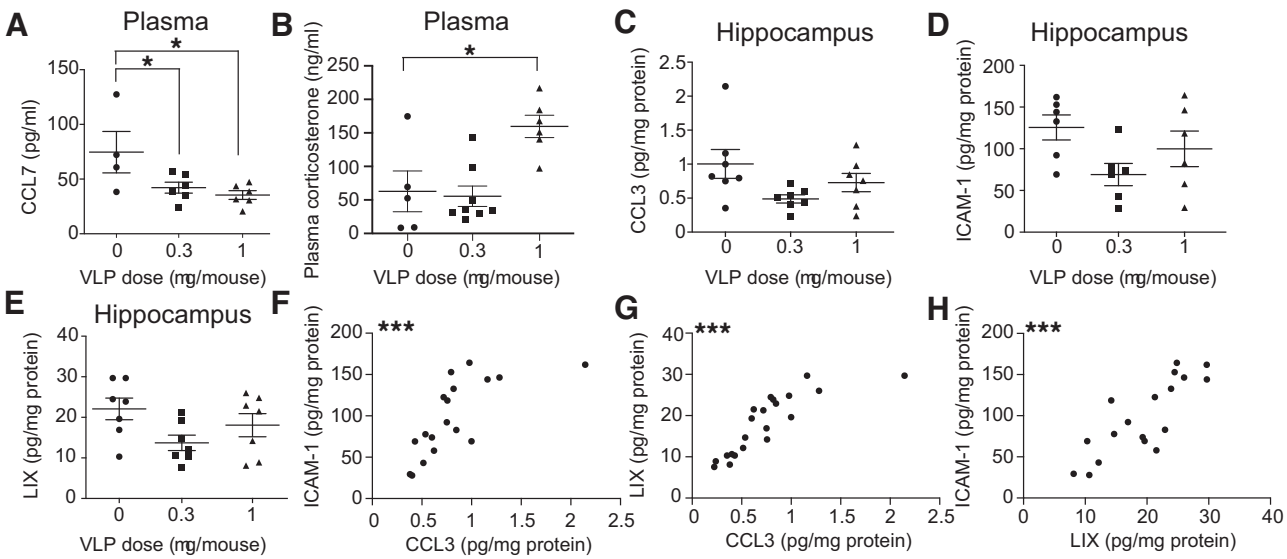

Fig. 1 | Selection of VLP dose to affect the mouse immune system. A VLP injections showed a significant effect on the plasma levels of CCL7 ($F = 4.703$, $p = 0.0291$, all tests in (**A**–**E**) are one-way ANOVAs. All *post hoc* comparisons were conducted using Dunnett's correction for multiple comparisons). **B** Injection of 1 μg VLPs caused a significant increase in plasma corticosterone levels, while injection of 0.3 μg caused no significant change compared to the vehicle injection ($F = 8.512$, $p = 0.003$). **C** Increasing the VLP exposure levels resembled a U-shaped effect on hippocampal CCL3 levels ($F = 2.976$, $p = 0.07$). **D** Similar to (**C**), increasing VLP exposure levels resembled a U-shaped effect on hippocampal ICAM-1 levels ($F = 2.798$, $p = 0.09$). **E** Similar to (**C**, **D**), increasing VLP exposure levels resembled a U-shaped effect on hippocampal LIX levels ($F = 2.807$, $p = 0.09$). **F** Positive correlation between hippocampal levels of ICAM-1 and CCL-3 ($r = 0.7115$, $p = 0.0009$, Pearson's correlation). **G** Positive correlation between hippocampal levels of LIX and CCL-3 ($r = 0.8324$, $p < 0.0001$, Pearson). **H** Positive correlation between hippocampal levels of ICAM-1 and LIX ($r = 0.8184$, $p < 0.0001$, Pearson). $n = 19$ mice; VLP 0 μg: $n = 5$ mice; VLP 0.3 μg: $n = 8$; VLP 1 μg: $n = 6$). $^{*}p < 0.05$; $^{**}p < 0.01$; $^{***}p < 0.001$.

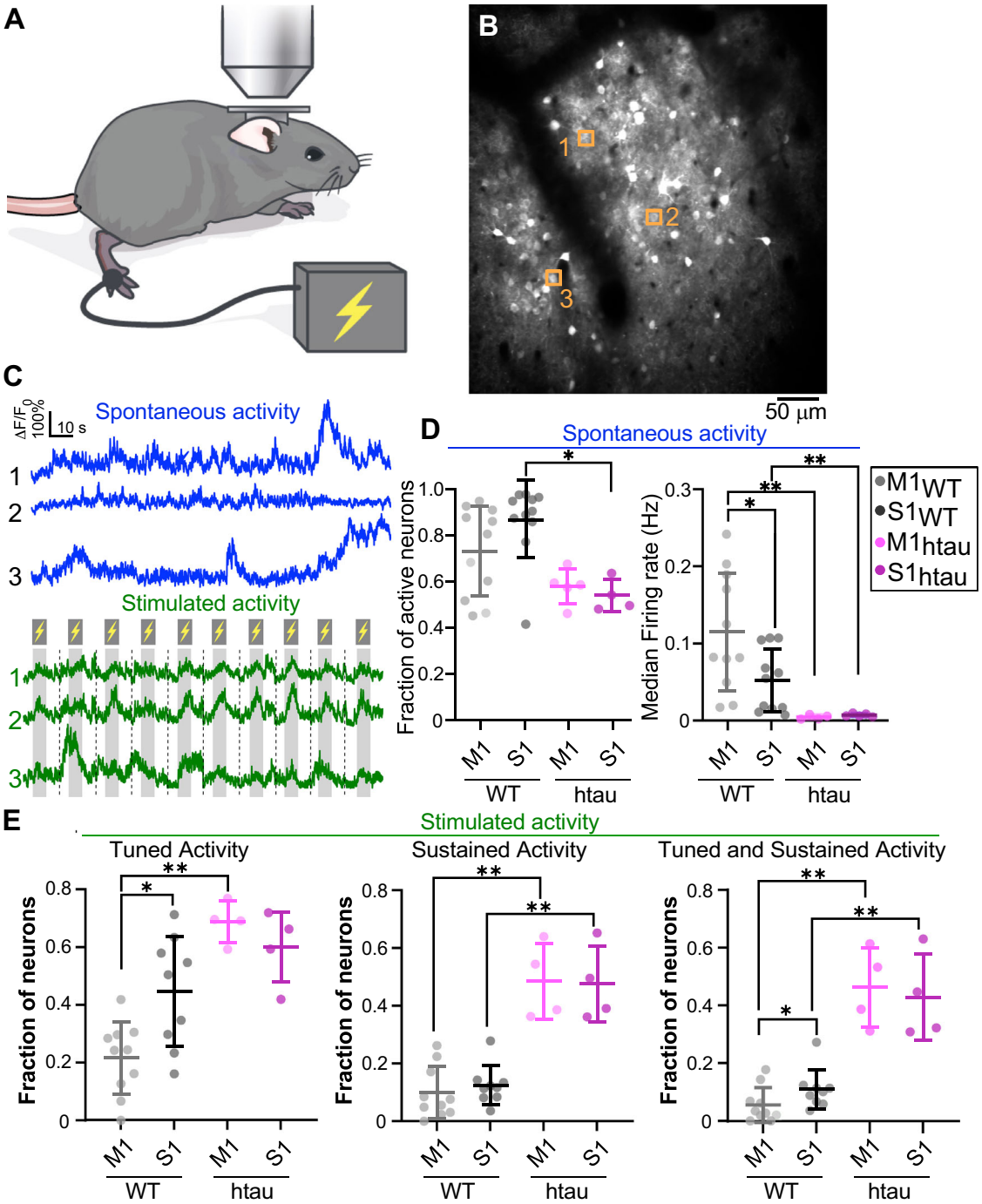

same $S1_{HL}$ and $M1_{limbs}$ neurons to a series of hindlimb paw stimulations (stimulated activity; see Methods), were also recorded in both WT and htau mice (Fig. 2A–C, see Methods for details). These two genotypes showed different brain activity patterns. The fraction of neurons that fired spontaneously and their median firing rates were significantly higher in WT mice than in htau mice (Fig. 2D). In contrast, the fractions of neurons that significantly increased their firing during paw stimulation or that maintained significantly higher jGCaMP7s fluorescence levels after the end of the stimulation period than their baseline fluorescence levels (tuned or sustained activity neurons, respectively), as well as the fraction of neurons that exhibited both tuned and sustained activity, were significantly higher in htau than WT mice (Fig. 2E). There was no significant difference between the $\Delta F/F_0$ stimulation response magnitude between the brain regions and genotypes. Finally, in WT mice, but not htau mice, the median spontaneous firing rate of S1 neurons was significantly higher than that of M1 neurons (Fig. 2D), which was also the case for the fraction of S1 neurons that were tuned to paw stimulation or showed both tuned and sustained activity (Fig. 2E). Due to these fundamental differences in brain activity patterns between the two mouse genotypes, the analysis of VLP exposure effect on each line was performed separately in the following sections. In addition, since no significant changes were found between M1 and S1 neuronal activity patterns in htau mice (Fig. 2D, E), data from these regions were merged for the following analyses.

Short-term increases in firing properties following exposure to SARS-CoV-2 VLPs

Following the recordings of baseline neuronal activity, both WT and htau mice were randomly assigned to 2 groups and received a single IP

Fig. 2 | Recording of baseline spontaneous and stimulated activity in WT and htau mice. A Schematic illustration of the experimental setup. Mice were lightly anesthetized, sedated, and received trains of electric stimuli to their hindlimbs while neuronal activity from their motor and somatosensory cortices was recorded using two-photon microscopy. **B** Example image of S1 neurons expressing jGCaMP7s. scale bar, 50 μm. **C** Examples of spontaneous and stimulated activity traces (blue and green traces, respectively) from the cells indicated by orange boxes in panel (**B**). Gray bars and lightning signs indicate the times where the paw stimulation was given to the mouse, while dashed vertical lines indicate the separation between stimulation cycles. **D** Comparison of the fraction of neurons that fired action potentials during the spontaneous activity recordings in S1 and M1 out of all recorded neurons in the same brain region (active neurons), and the median firing rate of the active neurons. The fraction of active neurons was significantly higher in the S1 region of WT mice than that of htau ($p = 0.018$, Wilcoxon Rank Sum Test). For the median firing rate panel, each dot is the median across all the recorded active neurons from the same brain region of one mouse. WT median firing rates in S1 and M1 regions were significantly higher than the respective regions in htau mice ($p = 0.0015$ and 0.0018, respectively, Wilcoxon Rank Sum Tests). In addition, the median firing rate in M1 of WT mice was significantly higher than that in S1 ($p = 0.02$, Wilcoxon Signed-Rank Test). **E** Comparison of the stimulated activity metrics shows a significant increase in htau vs. WT fraction of M1 neurons that increased their activity during paw stimulation (tuned activity), after the stimulation (sustained activity), or showed both tuned and sustained activity (comparing M1 neurons between WT and htau: $p = 0.002$ for the three comparisons; Wilcoxon Rank Sum Tests). A similar comparison for the S1 region showed that htau mice had a higher fraction of sustained activity neurons as well as a higher fraction of neurons with both tuned and sustained activity (comparing S1 neurons between WT and htau: left panel: $p = 0.15$, middle and right panels: $p = 0.003$; Wilcoxon Rank Sum Tests). In addition, for WT mice, a higher fraction of S1 than M1 neurons was tuned and showed both tuned and sustained activity ($p = 0.016$ for both comparisons, Wilcoxon Signed-Rank Tests). 49–708 and 59–1172 neurons were recorded to calculate each data point in (**D**) and (**E**), with median values of 355 and 513 neurons, respectively. For the Wilcoxon Rank Sum Tests data from $n = 12$ WT and 6 htau mice were used in (**D**) and $n = 12$ WT and 5 htau mice in (**E**). For the Wilcoxon Signed-Rank Tests we used $n = 10$ M1 and S1 pairs from WT and 3 pairs from htau mice for (**D**); and $n = 7$ pairs from WT and 3 pairs from htau mice for (**E**). For both (**D**, **E**), each dot shows data from one mouse, horizontal bars are the mean per brain region, and error bars span the standard deviation. $^{*}p < 0.05$; $^{**}p < 0.01$.

injection of 0.3 μg VLPs or the same volume of vehicle solution (VLP group: 6 WT mice, 3 males and 3 females, and 3 htau mice: 2 males and 1 female; vehicle group: 6 WT mice, 3 males and 3 females, and 3 htau mice: 2 males and 1 female). Recording of brain activity started one hour after the IP injection and continued for an additional six weekly recordings. When analyzing the changes in brain activity during baseline recording, the day of injection and the following week (short-term effects) in WT mice, there was a respective mean increase of up to 200% and 105% in M1 and S1 stimulus-evoked response magnitudes following VLP exposure, which was not observed in the respective vehicle groups, indicating a short-term change in neuronal firing properties (Fig. 3A). Comparing the short-term changes in the fraction of tuned neurons in each brain region showed differences across the vehicle and VLP groups and an increase of 30–80% over time for the VLP group (Fig. 3B). Similarly, there was a significant short-term increase of 85–125% in the fraction of neurons with sustained activity and an increase of 95–290% in the fraction of neurons with both tuned and sustained activity for the VLP group compared to baseline. The magnitudes of these increases were generally higher in the M1 region than the S1 region, which started with higher baseline levels (Fig. 3B–D).

Measuring the same functional metrics in htau mice revealed different results. Similar to WT mice, the neuronal response magnitude following paw stimulation of htau mice showed a significant increase of up to 310% following exposure to VLP (Fig. 3E). Similarly, a significant increase was detected in the fractions of tuned, sustained, and tuned and sustained neurons, which brought their values close to the maximal possible value of 1 (Fig. 3F–H. Tuned neurons: a mean increase from 0.62 ± 0.12 during baseline recordings to 0.92 ± 0.07 one week after VLP exposure; sustained activity neurons: from 0.46 ± 0.13 to 0.90 ± 0.05; neurons with both tuned and sustained activity: from 0.42 ± 0.15 to 0.88 ± 0.07). Interestingly, htau mice also showed additional changes in spontaneous neuronal activity patterns that were not apparent in WT mice (Fig. 3I–L). There was a significant increases of 55% in the fraction of active neurons and of 370% in their median firing rates between baseline recordings and the week after VLP exposure (Fig. 3K, L; no significant changes were found in the same parameters for WT mice, Fig. 3I, J). These increases were not limited to the VLP group, and similar increases were evident in the htau vehicle group, but not in WT vehicle mice (Fig. 3I–L). These measurements indicate that systemic VLP exposure leads to short-term increases in neuronal firing properties in response to paw stimulation in both WT and htau mice; however, htau mice showed higher susceptibility to this exposure than WT mice, which was evident by the magnitude of increases in stimulated activity metrics, increases in spontaneous firing metrics, and detected increases in the vehicle group.

Long-term changes in neuronal activity following VLP exposure

To identify and compare long-term stimulated activity changes between WT and htau mice, the 6-week post-exposure recording data were grouped into early-term (exposure day and the following week), mid-term (weeks 2–3 after exposure), and late-term measurements (weeks 4–6 after exposure; same mice and groups as for the short-term recordings). The response magnitude of WT mice significantly increased in the early time after VLP exposure and then returned to similar levels like the baseline values. The vehicle group values remained close to the baseline levels throughout all recordings (Fig. 4A). Interestingly, the fraction of tuned neurons, the fraction of sustained activity neurons, and neurons with both tuned and sustained activity of the VLP group showed an early-term increase, which was followed by a partial decay to an intermediate level that was higher than baseline (Fig. 4B–D). Overall, WT mice showed substantial short-term increases, which reached their peaks approximately one week after exposure to VLPs (Fig. 3A–D). Longer-term effects of VLP exposure on brain activity were evident during the 6 post-exposure weeks that were monitored, but their magnitude was lower than the short-term effects.

For htau mice, we identified a different pattern of long-term effects following VLP exposure than in WT mice. For all measured metrics, there were no significant changes among the VLP and vehicle groups, but there were significant changes over time. The response magnitude of the recorded neurons was increased early after the exposure for both the VLP and vehicle groups, and then significantly decreased during the mid- and late-term (Fig. 4E–H). Interestingly, the mean response magnitude of both the VLP and vehicle groups in the late-term was higher than before the exposure (Fig. 4E), while the mean fractions of tuned, sustained, and neurons with both tuned and sustained activity were lower (Fig. 4F–H), although these differences were not significant.

When analyzing changes in the spontaneous activity characteristics of WT and htau mice, we found no significant changes in WT mouse activity patterns (Fig. 4I, J). For htau mice, there was an increase for both the VLP and vehicle groups during the early term after the exposure. However, while there was a return of the vehicle groups to levels close to baseline, the VLP groups decreased from the early peak but remained elevated compared to the baseline levels with a significant difference among the two groups (Fig. 4K, L).

Discussion

This work investigates the longitudinal effects of VLP exposure on neuronal activity patterns in the mouse primary motor and somatosensory cortices. These regions receive sensory input via the thalamus[31], allowing cortical network processing to be studied using an externally controlled and relatively simple stimulus. The use of VLPs enabled studying such effects while reducing most of the risk associated with the replicating SARS-CoV-2 virus

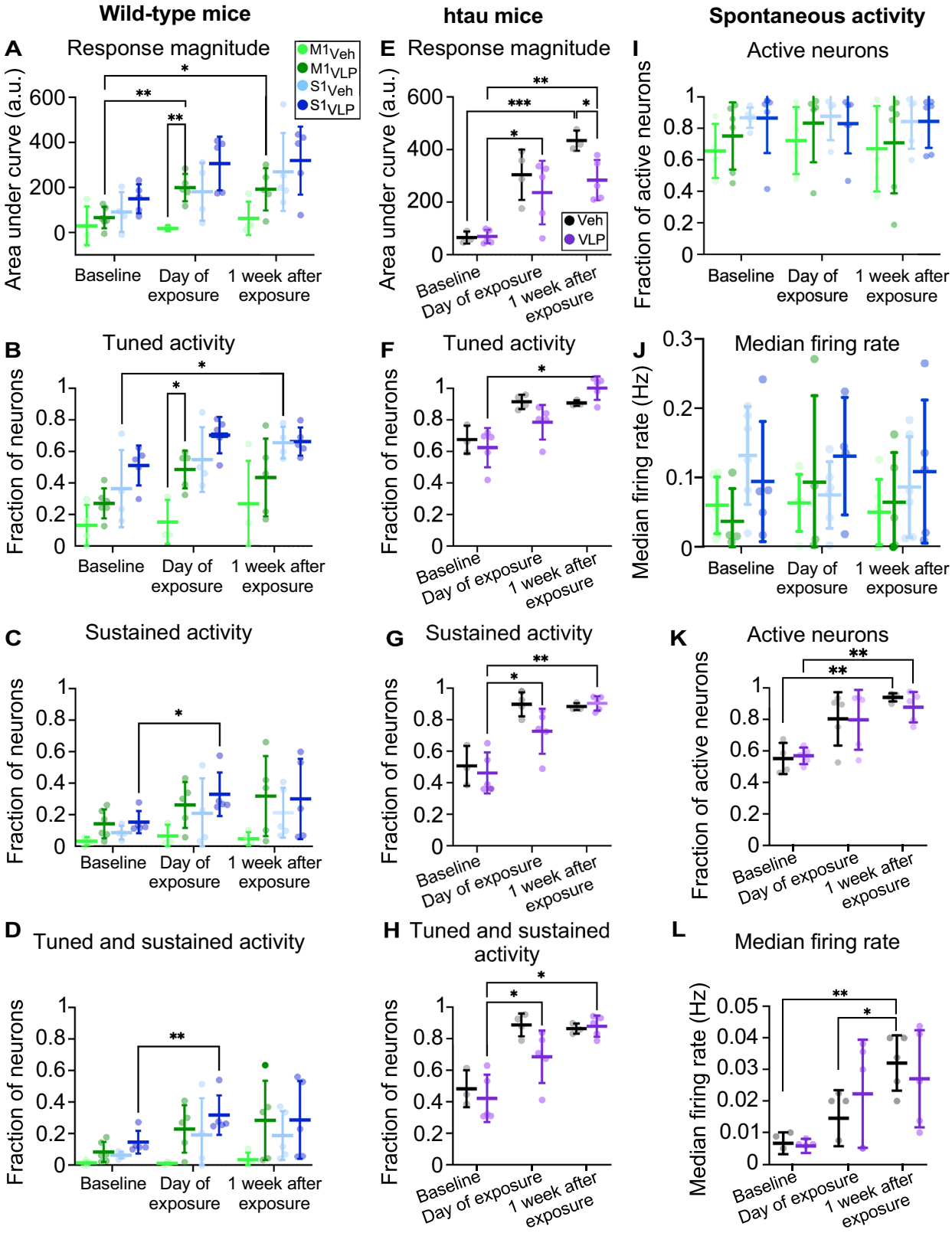

and its derivatives. This simplified framework lowered barriers to conducting more advanced imaging studies, such as longitudinal two-photon microscopy recordings of single-neuron activity in vivo, which would have been considerably more challenging to perform otherwise. By recording cortical activity for six consecutive weeks following exposure to VLP or vehicle, we identified both short- and long-term changes in stimulus-evoked and spontaneous activity patterns and explored differences between WT and htau mice.

We tested the effects of different VLP doses on the mouse immune system and inflammatory responses, and selected the 0.3 μg/mouse dose, which elicited a strong immune response without alterations in plasma corticosterone levels (Fig. 1A, B). Next, we studied the effect of VLP

Fig. 3 | Short-term changes in neuronal firing properties following exposure to VLPs. Panels **A**–**D** summarize the findings from recording stimulated neuronal activity in WT mice. **A** Repeated recordings from the same mice before, on the day of VLP/vehicle injection, and in the following week, showed a significant short-term increase in the area under the curve of the measured fluorescence response magnitude. We detected significant changes in M1 neuronal responses to hindlimb stimulation between VLP and vehicle groups on the VLP exposure day, as well as a significant increase in the VLP group response magnitude over time. **B** A significant increase in the fraction of tuned S1 neurons was found following VLP exposure, as well as a significant difference between the M1 vehicle and VLP groups on the exposure day. **C** Same comparison for the fraction of neurons that exhibited sustained activity showed significant increase in S1 neurons following exposure to VLP. **D** Same comparison for the fraction of neurons that exhibited both tuned and sustained activity patterns showed a significant increase in S1neuronal metrics following VLP exposure. For the VLP group, we note that following VLP exposure, M1 levels increased more than S1 levels to the point that they reached similar levels, closing most of the gap that existed during baseline recording (Fig. 2). Panels **E**–**H** summarize the finding from recording stimulated neuronal activity from htau mice. **E** Measuring the area under the curve of the acquired fluorescence response magnitude to hindlimb repeated stimulation of htau mice showed significant increases of 235–430% over time, with a larger increase in the vehicle group a week after exposure. **F** A significant increase in the fraction of tuned neurons over time was found for the VLP group, without a significant difference among the groups. **G** The fraction of VLP neurons that exhibited sustained activity also showed a significant increase over time without a significant change between the two groups. **H** Similar to (**F**, **G**), the fraction of neurons that exhibited both tuned and sustained activity showed a significant increase over time without a significant difference between the two groups. Panels **I**, **J** and **K**, **L** summarize the finding from recording spontaneous neuronal activity from WT and htau mice, respectively. **I**, **J** Repeated measures of changes in the spontaneous activity of WT neurons showed no significant changes over time or changes across the different groups. **K**, **L** Repeated measures of changes in the spontaneous activity of htau neurons showed a significant increase of up to 70% over time in the fraction of neurons that fired action potentials during the recording and of 390% in their median firing rates. Each dot shows the fraction of neurons with at least one detected action potential from all recorded neurons in the same brain region (**I**, **K**), or the median of the average firing rate across all active neurons within each region (**J**, **L**). All tests in (**A**–**L**) used mixed-effect models with restricted maximum likelihood and Tukey Honest Significant Difference *post hoc* comparisons. Data from $n = 4$–6 mice were used for each group in (**A**–**D**): 6 mice were included in the $M1_{VLP}$ group, 5 in $S1_{VLP}$, 4 in $M1_{Veh}$, and 4 in $S1_{Veh}$; 49–708 neurons were recorded to calculate each data point in (**A**–**D**), with a median value of 192 neurons. Data from $n = 5$ brain regions were used to calculate the data in (**E**–**H**), recorded from 5 S1 and M1 regions from 3 mice for the VLP group and 4 S1 and M1 regions from 2 mice for the vehicle group, 102–639 neurons were recorded to calculate each data point, with a median value of 206 neurons. Data from $n = 5$–6 mice were used for each group in (**I**, **J**): 6 mice were included in the $M1_{VLP}$ group, 6 in $S1_{VLP}$, 5 in $M1_{Veh}$, and 5 in $S1_{Veh}$; 19–1172 neurons were recorded to calculate each data point in (**I**, **J**), with a median value of 317 neurons. Data from $n = 5$ brain regions were used to calculate the data in (**K**, **L**), recorded from 5 S1 and M1 regions from 3 mice for the VLP group and 5 S1 and M1 regions from 3 mice for the vehicle group; 115–990 neurons were recorded to calculate each data point in (**K**, **L**), with a median value of 271 neurons. Horizontal bars and error bars show the mean ± std across all data points. $^{*}p < 0.05$; $^{**}p < 0.01$, $^{***}p < 0.001$. Values of all statistical tests and *p*-values may be found in Supplementary Tables 1 and 2.

exposure on mice and how it relates to the presence of the human tau protein. Tau is fundamentally involved in tauopathy disorders as well as considered to be central in AD progression. Tau expression levels depend upon the mouse age, which potentially may also affect its performance in various behavioral tests, although there have been mixed reports on this issue[16]. We studied mice that were 11–13 months old during recordings, which is an age range when substantial tau-related cellular and behavioral pathology have been reported for the htau line[15–18]. To the best of our knowledge, the measurements reported in this study are the first to be conducted in the context of exposure to SARS-CoV-2 VLPs.

Our data indicate several interesting findings. First, neuronal activity patterns of htau mice were significantly different than those of WT mice under baseline conditions. These differences may be attributed to the expected higher levels of human tau that is expressed in middle-aged htau mice[15]. The htau mice showed lower spontaneous firing rates, in agreement with previous findings using other tau-expressing mouse models[23,32,33]. These studies showed that increases in different forms of tau lead to reductions in neuronal firing, either during periods of resting or movement[32,33]. However, here we also found that the stimulus-evoked activity metrics of htau mice were higher than those of WT mice, but this was not due to increased response amplitudes (Fig. 2). This may suggest that tau expression affects spontaneous and stimulated activity differently, possibly by exerting distinct influences on the thalamocortical circuit involved in upstream stimulus processing versus local neurons that provide input to S1 and M1 neurons during spontaneous recordings. Importantly, modified experimental protocols, such as using different mouse tau lines and different experimental conditions, may contribute to differences in the reported findings between the current and previous studies. Moreover, we observed that middle-aged htau mice had lower survival rates than WT mice following the craniotomy required for this study. Consequently, fewer htau mice were included in this paper, which reduced the sample size and limited the statistical power of the longitudinal study. To partially address this limitation, we combined data from the S1 and M1 regions of htau mice for analysis. However, since these regions are functionally distinct, it is possible that region-specific differences were not detected due to the limited sample size or that similarities between these regions were given additional weight in the analysis.

Second, upon exposure to VLPs, both genotypes showed a short-term increase in the measured stimulus-evoked neuronal firing properties, but htau mice also showed changes in spontaneous activity patterns, as well as changes in response to the vehicle injection (Figs. 3 and 4). This may relate to a differential response of the htau mice to the IP injection and/or the weekly anesthesia and sedation procedure that was part of the imaging sessions. Increased depressive-like behavior and increased measures of anxiety were reported in htau mice[34], and the stress conditions associated with an IP injection and repeated anesthesia sessions may contribute to this difference between the WT and htau groups.

Finally, while WT mice showed long-term increases in the measured stimulus-evoked activity metrics, the htau mice showed a more complex repertoire of altered activity patterns. The measured metrics, both for stimulus-evoked and spontaneous activity, showed both increases and decreases with respect to their baseline levels. We hypothesize that the human tau protein expression in the htau mice affects the excitability of their cortical neurons (Fig. 2D, E). When these mice face a major insult, such as exposure to VLPs, their neuronal circuits are less stable and are easier to be altered compared to WT mice. Our findings also support the hypothesis that expression of the human tau protein makes the htau mice more vulnerable to VLP exposure, with more severe short- and long-term side effects compared to WT mice (Figs. 3 and 4). This may be similar to the increased vulnerability of patients with, or at higher risk of developing, neurodegenerative conditions, who are not only more susceptible to severe COVID-19 infection[35,36] but may also develop symptoms of long COVID (Post-acute Sequelae of SARS-CoV-2 infection)[37]. Various immune mediators are altered in the response to SARS-CoV-2[38–42] and future efforts will be required to assess the role of central inflammation in the effects of VLPs on brain function.

Methods

All surgical and experimental procedures were conducted in accordance with protocols approved by the Lerner Research Institute and Oregon Health and Science University Institutional Animal Care and Use Committees and Institutional Biosafety Committees. We have complied with all relevant ethical regulations for animal use.

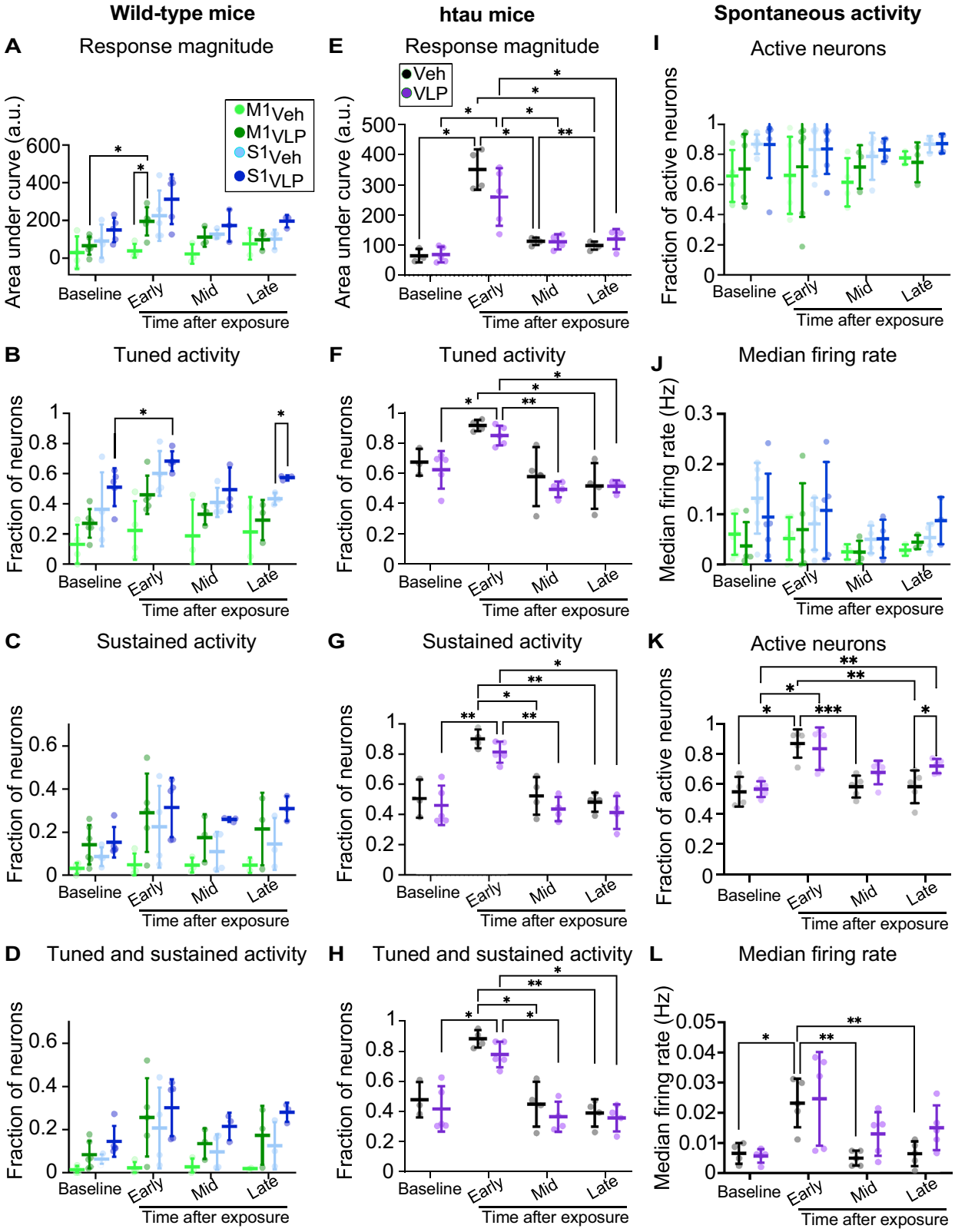

Preparation of VLPs

Plasmid expression vectors encoding each of the SARS-CoV-2 N, M, E, and S proteins were constructed by standard cloning methods, using synthesized codon optimized sequences, as reported[9]. M, E, N, and S plasmids were transfected at a ratio of 5:1:5:1 into suspension-grown Expi293F cells using Expifectamine reagent (ThermoFisher). Culture supernatant was passed through a 0.45 μm filter, followed by ultracentrifugation through a 20% sorbitol cushion at 30,000 rpm for 2 h. The pellet was resuspended in 1/100th original volume of phosphate-buffered saline (PBS). VLP structure assessed by transmission electron microscopy of negatively-stained samples.

Fig. 4 | Long-term changes in firing properties following exposure to VLPs. **A** Data were divided into baseline (pre-exposure) and post-exposure times: early (mean of same-day and the following week), mid (mean of 2–3 weeks post-exposure), and late (mean of 4–6 weeks post-exposure). The median area under the curve of the neuronal response amplitudes following paw stimulation showed significant changes among the VLP and vehicle groups and over time. Interestingly, for the VLP group, there was a short-term increase following the exposure to VLP and then a non-significant decay. **B** The fraction of tuned neurons in the VLP group was higher than in the vehicle group upon VLP exposure and remain higher during the exposure period. Significant differences were found for the S1 neurons. **C** The fraction of neurons with sustained activity showed similar trends to the change in tuned neurons, but without a significant difference between individual recordings (significant time and group effects were found, see Supplementary Table 3). **D** The fraction of neurons that exhibited both tuned and sustained activity showed similar trends to the changes in (**B**, **C**), but without significant differences between individual recordings (significant time and group effects were found, see Supplementary Table 3). **E** The median area under the curve of the neuronal response amplitudes following paw stimulation in htau mice showed a large early-phase increase and then a significant decrease to values that remained higher than baseline levels. **F** The fraction of tuned neurons showed a significant increase in the early phase after exposure to VLP and then a significant decreased to levels lower than the baseline without a significant difference between the groups. **G**, **H** The fraction of neurons that exhibited sustained activity and the fraction of neurons that exhibited both sustained and tuned activity showed significant temporal changes with an early-phase increase and then a return to levels lower than baseline. **I** There were no significant changes between the recorded WT groups for the fraction of active neurons (the neurons that fired at least one action potential during spontaneous activity recording). **J** There were no significant changes between the median spontaneous firing rates of active neurons for the WT groups (a significant time effect was found, see Supplementary Table 3). **K** A significant change over time and differences among the VLP and vehicle groups were found for the fraction of active neurons during spontaneous activity for htau mice. Following a short-term increase, the fraction for the VLP group remain elevated compared to the vehicle group. **L** The median firing rate of active neurons during recording of spontaneous activity showed a similar pattern to (**I**). All tests in (**A**–**L**) used mixed-effect models with restricted maximum likelihood and Tukey Honest Significant Difference *post hoc* comparisons. Data from $n = 4$–6 mice were used for each group in (**A**–**D**): 6 mice in the $M1_{VLP}$ group, 5 in $S1_{VLP}$, 4 in $M1_{Veh}$, and 5 in $S1_{Veh}$; 21–708 neurons were recorded to calculate each data point in (**A**–**D**), with a median value of 168 neurons. Data from $n = 5$ brin regions were used to calculate the data in (**E**–**H**), recorded from 5 S1 and M1 brain regions from 3 mice for the VLP group and 4 S1 and M1 regions from 2 mice for the vehicle group, 67–639 neurons were recorded to calculate each data point, with a median value of 190 neurons. Data from $n = 5$–6 mice were used for each group in (**I**, **J**): 6 mice were included in the $M1_{VLP}$ group, 6 in $S1_{VLP}$, 5 in $M1_{Veh}$, and 5 in $S1_{Veh}$;19–1172 neurons were recorded to calculate each data point in (**I**, **J**), with a median value of 349 neurons. Data from $n = 5$ brain regions were used to calculate the data in (**K**, **L**), recorded from 5 S1 and M1 regions from 3 mice for the VLP group and 5 S1 and M1 regions from 3 mice for the vehicle group; 56–990 neurons were recorded to calculate each data point in (**K**, **L**), with a median value of 206 neurons. Horizontal bars and error bars show the mean ± std across all data points. $^{*}p < 0.05$; $^{**}p < 0.01$. Values of all statistical tests and *p*-values may be found in Supplementary Tables 3 and 4.

Dose-response curve for the effects of VLPs on the Hypothalamic-Pituitary-Adrenal axis and analysis of cytokines and chemokines in plasma and the hippocampus

Nine-month-old C57BL/6J WT mice ($n = 19$) were injected with VLPs (0 [$n = 5$], 0.3 [$n = 8$], or 1 [$n = 6$] μg, IP). Vehicle media without VLPs but otherwise processed the same way was used for the 0 dose injections. One hour later, blood was collected from the mandibular vein in unanesthetized mice with 0.5 M EDTA and centrifuged at 40,000 × *g* for 10 min at 4 °C to collect plasma, as described[43]. Twenty-four hours later, the mice were euthanized by cervical dislocation and plasma and hippocampal cytokines and chemokines levels were analyzed using a Luminex panel (46PLEX, Mouse Magnetic Luminex Assay). Hippocampi were homogenized in a lysis buffer consisting of 1 M Tris-Cl, 6 M NaCl, 10% SDS, and 0.5 M EDTA, 1% Triton-X, and protease inhibitor (Roche, Sigma Aldrich, catalog #11836170001, St. Louis, MO). Total protein amounts were determined with a BCA protein assay kit (Pierce, Thermo Scientific, catalog #23225, Waltham, MA). Plasma corticosterone was analyzed using a radioimmune assay kit (MP Biomedicals, Irvine, CA). Intra-assay coefficient of variation was 10% and the inter-assay coefficient of variation was 7%.

Surgical preparation of mice

We used C57BL/6J mice and mice that express the human tau protein[15] (WT and htau mice, JAX strain #000664 and #005491, respectively). The mice were housed under standard vivarium conditions with *ad libitum* access to food and water and a 12-h light/12-h dark cycle. All experiments are conducted during the light phase. All mice were implanted with cranial windows above their left S1 and M1; 10 months old at the time of surgery; $n = 12$ C57BL6/J mice, 6 males and 6 females; $n = 6$ htau mice, 4 males and 2 females). The window was placed 1 mm anterior to 4 mm posterior to Bregma, 0.5–3.5 mm lateral to midline, similar to previously-published works[44–46]. Mice were first anesthetized using isoflurane (3% for induction, 1.5% during surgery), the scalp skin was cut and removed, and a rectangular craniotomy was drilled (OMNIDRILL35, World Precision Instruments). An adeno-associated virus (AAV) solution expressing jGCaMP7s under the *human synapsin* promoter (Addgene catalog number 104487-AAV1, $2.7{*}10^{13}$ GC/ml, diluted 1:10 with saline) was injected into the cortex according to mouse brain atlas coordinates[30] (Injection locations anterior/lateral to bregma: M1: two locations, 0.5/−1 mm and −0.5/−1.25 mm, the first location corresponds to the vibrissa and neck, the second location between the forelimb and hindlimb regions ($M1_{VN}$ and $M1_{limbs}$, respectively) according to a microstimulation study[47]; S1: two locations, −0.5/−1.9 mm and −1.75/−2.5 mm, which correspond to S1 hindlimb and S1 barrel field regions (S_{HL} and S_{BF}, respectively). Forty nL of virus solution were injected per location, 250 and 500 μm under the pia using a 1 mm-diameter pulled and beveled glass micropipette (P-100 puller and BV-10 beveller, Sutter). The craniotomy was covered with a glass window (two-layer cranial window: $5 \times 3 \times 0.17$ mm^3 glass glued to a $6 \times 3 \times 0.17$ mm^3 glass; Tower Optical) and secured to the skull bone using ethyl cyanoacrylate glue (Krazy Glue) and dental cement (Contemporary Ortho-Jet, Lang Dental). A custom stainless-steel head post was also cemented to the skull using the same dental cement. Mice were given post-operative care for pain management and 3–4 weeks for recovery before the beginning of recordings.

VLP exposure

A VLP dose of 0.3 μg/mouse was injected intraperitoneally (IP) one hour before the initiation of the recording session on the treatment day. Vehicle mice were injected with an identical volume of the vehicle solution one hour prior to the initiation of the imaging session on the same day.

Recording of brain activity

Similar to previous works[44,45,48–51], mice were lightly anesthetized using isoflurane (0.5%), sedated using intramuscular injection of Chlorprothixene Hydrochloride (30 μl of 0.33 mg/ml solution, Spectrum Chemical MFG Corp), and were kept in the dark on a 37 °C heating pad for at least 30 min before the start of recording. The jGCaMP7s injection spot in each brain region was identified for each mouse and an attempt to consistently record from the same fields of view (FOVs) was made. In case the same FOV could not be identified, the recording was conducted from a similar depth under the brain surface as in the previous recordings (see example images in Supplementary Figs. 1, 2). We first recorded spontaneous brain activity using a Bergamo II two-photon microscope (ThorImage 4.1 software, Thorlabs) equipped with resonant-galvo scanners (1024 × 1024 pixels, 15 frames/sec, 600 × 600 μm^2 FOV) and a GaAsP PMT detector. jGCaMP7s signal was excited using 950 nm light (Insight X3, Spectra-Physics) and a 16x objective with 0.8 NA (Nikon CFI LWD). The fluorescence signal was collected using a 525/50 emission filter (Chroma). For monitoring spontaneous activity, each FOV was recorded for 200 sec. Typically, two FOVs were recorded from all of the S1 and M1 regions that showed jGCaMP7s

expression in each mouse. Then, a thin needle electrode was attached to mouse hindlimb (29-gauge needle electrode, AD Instruments) and connected to a pulse stimulator (A-M Systems, model 2100). The recording was divided into 10 cycles. Each cycle started by 5 sec of baseline recording, followed by 5 sec of paw stimulation with 25 electric stimuli. Each stimulus consisted of a 1.5 mA square amplitude pulse of 100msec duration, which was followed by 100msec without stimulus, for a total of 5 sec. The recording cycle was concluded by acquiring additional 5 sec of brain activity without stimulation. The stimulation and the imaging clocks were synchronized using ThorSynch software. A delay of 5 sec without recording separated subsequent cycles. Typically, 2 FOVs per brain region were recorded from the $M1_{limbs}$ and the S_{HL} regions from each mouse in all recording sessions. Mice were recorded for 2–3 baseline recording sessions before they were exposed to VLP/vehicle. Then, they were recorded on the exposure day, with the recording session starting 1 h after the IP injection. Afterwards, the mice were recorded once a week for additional 6 weeks. All recording sessions were identical. In case we could not identify jGCaMP7s expression in a specific brain region of a mouse, this brain region was not included in the study. In case the quality of imaging deteriorated in a specific brain region over time, for example due to bone growth under the cranial window, we recorded from this region as long as we could identify single cells and then excluded the rest of the recording from the study. In case both the $S1_{HL}$ or $M1_{limbs}$ regions could not be recorded from a mouse, no stimulated or spontaneous activity data were recorded from the respective region, but spontaneous activity recordings continued from the other regions.

In 4 recordings of stimulated activity from 4 different mice, one of the stimulation cycles could not be synchronized to the imaging data since the ThorSynch file was corrupted. For these recordings, we calculated the same analysis using 9 stimulation cycles. In 2 recording of spontaneous activity from 2 mice, the last 22 and 26 frames were not saved properly, and we ran the analysis on the properly-saved frames. The recording order of mice was not controlled.

Mice are inspected weekly for weight loss and changes in fur condition or posture, which may indicate poor health. No mice were excluded from the study due to poor health.

Brain activity data analysis

Analysis was based upon custom MATLAB scripts (MathWorks), similar to our previously-published data[44,50,51]. Raw fluorescence movies were registered using the TurboReg plug-in in ImageJ to correct small movements[49,52]. Regions of interest (ROIs) corresponding to all identifiable somata were labeled using CellPose software[53]. Cells with nuclear-filled fluorescence signal were excluded from the analysis to eliminate potential side effects of GCaMP overexpression[49]. Recorded data were inspected for low expression of jGCaMP7s, movement artifacts, or low image quality, and we excluded recorded movies with such issues from the analysis. We note that the htau mice express low level of background GFP signal, and cells with low (<5%) contrast of the somatic jGCaMP7s signal with the surrounding background were also excluded from the analysis. Fluorescence signal from all pixels of each ROI were averaged to calculate the time-dependent fluorescence signal (F) and were corrected for neuropil contamination[54] using r = 0.7, baseline signal (F_0) for each neuron was estimated as the mean value of F three seconds prior to the initiation of the paw stimulation for stimulated data, or as the median fluorescence value for spontaneous recordings. The single-cell fluorescence change was calculated using the formula: $\Delta F/F_0 = (F–F_0)/F_0$. Action potential (AP) firing number and timing were estimated for spontaneous activity using the SpikeML algorithm[55] that extracted these values from the single cell $\Delta F/F_0$ using the following jGCaMP7s parameters[48] (1AP amplitude = 35%, decay time = 600 msec, Hill coefficient = 2.49). SpikeML output was used to calculate the fraction of active neurons (neurons with at least one identified AP during recording) and the average cellular firing rates and to compare changes across recording sessions. For analyzing short-term changes, we compared measurements from baseline (mean of recordings for mice with more than one baseline recording), the exposure week, and the following week, while for identifying long-term changes, we averaged the measured values across the early time after exposure (same day and the following week), middle (weeks 2–3 after exposure), and late (weeks 4–6 after exposure). When spontaneous activity was recorded from more than one S1 or M1 sub-regions, we averaged the results from all recorded FOVs and sub-regions for presenting the data in Figs. 2–4.

For quantifying the stimulated neuronal activity, we calculated the following values:

F_{base} – average fluorescence during the 3 sec before each paw stimulation started.

F_{stim} - average fluorescence during the 5 sec of paw stimulation plus the following 1 sec to compensate for jGCaMP7s slow kinetics.

F_{decay} - average fluorescence during the 3 sec starting 1 sec after the end of paw stimulation until 4 sec after the end of the paw stimulation. For recording of each FOV, we ran 10 cycles of paw stimulation, with 5 sec of 5 stimuli/sec in each, therefore, F_{base}, F_{stim}, and F_{decay} were vectors containing 10 values each. For defining whether a neuron is tuned, we ran a paired Student's t test ($p = 0.01$) between the F_{base} and F_{stim} vectors. For defining whether a neuron has sustained activity, we ran a paired Student's t test ($p = 0.01$) between F_{base} and F_{decay}. A cell that passed as significant in both tests was defined as a neuron with both tuned and sustained activity. Next, we defined the median area under the curve (AUC) as the median of the sum of the $\Delta F/F_0$ values during 6 sec in each of the 10 stimulus cycles (5 sec of each stimulus cycle + additional 1 sec after the end of each cycle). This value was divided by 2 and then we subtracted the median of the sum of $\Delta F/F_0$ values during the 3 sec of baseline period prior to the first stimulus.

Statistics and reproducibility

Statistical analysis was conducted using GraphPad Prism (version 10.1.2) and Matlab. For the Luminex and plasma corticosterone analysis, one-way ANOVAs with Dunnett's *post hoc* tests were used. To assess relationships between hippocampal chemokine levels, Pearson's correlations were used. For analyzing the differences between baseline activity levels in Fig. 2, we used non-parametric comparisons (Wilcoxon Rank Sum Tests and Wilcoxon Signed-Rank Tests). For analyzing the repeated neuronal activity measurements, mixed-effect models with restricted maximum likelihood and Tukey Honest Significant Difference *post hoc* tests ($p \le 0.05$) were used to identify changes between groups (VLP and vehicle) and time points. Data from WT and htau mice were analyzed separately due to the changes among these groups that were apparent during baseline recordings. Significant *post hoc* comparisons were shown only for comparing the same brain region across different times or for comparing differences between the VLP and vehicle groups for the same brain region. All statistical tests were two-sided.

The sample size was defined based on a-priori power analysis, which was based on data from other disease models. The numbers of samples for each statistical test are defined at the bottom of each figure legends. There were no replicated recordings in this study. Analysis of the data in Figs. 2–4 was done by a person who were blinded to which group (VLP or vehicle) the mice belonged. No other blinding was used in the study.

Reporting summary

Further information on research design is available in the Nature Portfolio Reporting Summary linked to this article.

Data availability

The data calculated from the raw recordings as well as the Prism file used for statistical analysis are available in Figshare repository https://doi.org/10.6084/m9.figshare.29238128[56]. Raw two-photon microscopy movies and synchronization files are available from the corresponding author upon reasonable request.

Code availability

Custom MATLAB scripts that were used for data analysis are available at Figshare repository https://doi.org/10.6084/m9.figshare.29238128.

Received: 26 November 2024; Accepted: 23 June 2025;
Published online: 03 July 2025

References

1. Partiot, E. et al. Brain exposure to SARS-CoV-2 virions perturbs synaptic homeostasis. *Nat. Microbiol.* **9**, 1189–1206 (2024).
2. Martínez-Mármol, R. et al. SARS-CoV-2 infection and viral fusogens cause neuronal and glial fusion that compromises neuronal activity. *Sci. Adv.* **9**, eadg2248 (2023).
3. Salvador, M. et al. SARS-CoV-2 spike protein reduces burst activities in neurons measured by micro-electrode arrays. *Ann. Med. Surg.* **85**, 3469–3476 (2023).
4. Golzari-Sorkheh, M., Weaver, D. F. & Reed, M. A. COVID-19 as a risk factor for Alzheimer's Disease. *J. Alzheimers Dis.* **91**, 1–23 (2023).
5. Wang, L. et al. Association of COVID-19 with new-onset Alzheimer's disease. *J. Alzheimers Dis.* **89**, 411–414 (2022).
6. Chen, F., Chen, Y., Wang, Y., Ke, Q. & Cui, L. The COVID-19 pandemic and Alzheimer's disease: mutual risks and mechanisms. *Transl. Neurodegener.***11**, 40 (2022).
7. Syed, A. M. et al. Rapid assessment of SARS-CoV-2–evolved variants using virus-like particles. *Science* **374**, 1626–1632 (2021).
8. Xu, R., Shi, M., Li, J., Song, P. & Li, N. Construction of SARS-CoV-2 Virus-Like Particles by Mammalian Expression System. *Front. Bioeng. Biotechnol.* **8** https://doi.org/10.3389/fbioe.2020.00862 (2020).
9. O'Niel, A. et al. Effects of COVID19 Virus-like particles on behavioral and cognitive performance of human apolipoprotein E targeted replacement mice. *Front. Immunol.* **15**, 1473366 (2024).
10. Syed, A. M. et al. Omicron mutations enhance infectivity and reduce antibody neutralization of SARS-CoV-2 virus-like particles. *Proc. Natl Acad. Sci.* **119**, e2200592119 (2022).
11. Yang, Q. et al. Role for *N*-glycans and calnexin-calreticulin chaperones in SARS-CoV-2 Spike maturation and viral infectivity. *Sci. Adv.* **8**, eabq8678 (2022).
12. Dubner, R. & Ruda, M. A. Activity-dependent neuronal plasticity following tissue injury and inflammation. *Trends Neurosci.* **15**, 96–103 (1992).
13. Jakubs, K. et al. Inflammation regulates functional integration of neurons born in adult brain. *J. Neurosci.* **28**, 12477–12488 (2008).
14. Miki, K. et al. Changes in gene expression and neuronal phenotype in brain stem pain modulatory circuitry after inflammation. *J. Neurophysiol.* **87**, 750–760 (2002).
15. Andorfer, C. et al. Hyperphosphorylation and aggregation of tau in mice expressing normal human tau isoforms. *J. Neurochemistry* **86**, 582–590 (2003).
16. Cho, J. D., Kim, Y. A., Rafikian, E. E., Yang, M. & Santa-Maria, I. Marked mild cognitive deficits in humanized mouse model of Alzheimer's-type tau pathology. *Front. Behav. Neurosci.* **15**, 634157 (2021).
17. Polydoro, M., Acker, C. M., Duff, K., Castillo, P. E. & Davies, P. Age-dependent impairment of cognitive and synaptic function in the htau mouse model of tau pathology. *J. Neurosci.* **29**, 10741 (2009).
18. Raber, J. et al. Effects of chronic secondhand smoke (SHS) exposure on cognitive performance and metabolic pathways in the hippocampus of wild-type and human tau mice. *Environ. Health Perspect.* **129**, 057009 (2021).
19. Di Primio, C. et al. Severe acute respiratory syndrome coronavirus 2 infection leads to tau pathological signature in neurons. *PNAS Nexus* **2**, pgad282 (2023).
20. Eberle, R. J. et al. Tau protein aggregation associated with SARS-CoV-2 main protease. *PLOS ONE* **18**, e0288138 (2023).
21. Ferrara, F. et al. Long COVID could become a widespread post-pandemic disease? A debate on the organs most affected. *Naunyn. Schmiedebergs Arch. Pharmacol.* **396**, 1583–1589 (2023).
22. Marwaha, B. Role of Tau protein in long COVID and potential therapeutic targets. *Front. Cell Infect. Microbiol.* **13**, 1280600 (2023).
23. Busche, M. A. et al. Tau impairs neural circuits, dominating amyloid-β effects, in Alzheimer models in vivo. *Nat. Neurosci.* **22**, 57–64 (2019).
24. Chung, S. J. et al. Association of Alzheimer's disease with COVID-19 susceptibility and severe complications: a nationwide cohort study. *J. Alzheimers Dis.* **87**, 701–710 (2022).
25. Dana, H. & Shoham, S. in *Handbook of neurophotonics* 55–80 (CRC Press, 2020).
26. Van Hartesveldt, C. in *The Hippocampus: volume 1: structure and development* 375-391 (Springer, 1975).
27. Cole, A. B., Montgomery, K., Bale, T. L. & Thompson, S. M. What the hippocampus tells the HPA axis: Hippocampal output attenuates acute stress responses via disynaptic inhibition of CRF+ PVN neurons. *Neurobiol. Stress* **20**, 100473 (2022).
28. Bui, T. M., Wiesolek, H. L. & Sumagin, R. ICAM-1: a master regulator of cellular responses in inflammation, injury resolution, and tumorigenesis. *J. Leukoc. Biol.* **108**, 787–799 (2020).
29. Rovai, L. E., Herschman, H. R. & Smith, J. B. The murine neutrophil-chemoattractant chemokines LIX, KC, and MIP-2 have distinct induction kinetics, tissue distributions, and tissue-specific sensitivities to glucocorticoid regulation in endotoxemia. *J. Leukoc. Biol.* **64**, 494–502 (1998).
30. Paxinos, G. & Franklin, K. B. *Paxinos and Franklin's the mouse brain in stereotaxic coordinates*. (Academic press, 2019).
31. Hooks, B. M., Lin, J. Y., Guo, C. & Svoboda, K. Dual-channel circuit mapping reveals sensorimotor convergence in the primary motor cortex. *J. Neurosci.* **35**, 4418–4426 (2015).
32. Marinković, P. et al. In vivo imaging reveals reduced activity of neuronal circuits in a mouse tauopathy model. *Brain* **142**, 1051–1062 (2019).
33. Wu, Q. et al. Increased neuronal activity in motor cortex reveals prominent calcium dyshomeostasis in tauopathy mice. *Neurobiol. Dis.* **147**, 105165 (2021).
34. Khan, K. M. et al. Human tau-overexpressing mice recapitulate brainstem involvement and neuropsychiatric features of early Alzheimer's disease. *Acta Neuropathol. Commun.* **11**, 57 (2023).
35. Li, C., Liu, J., Lin, J. & Shang, H. COVID-19 and risk of neurodegenerative disorders: a Mendelian randomization study. *Transl. Psychiatry* **12**, 283 (2022).
36. Dubey, S. et al. The Effects of SARS-CoV-2 infection on the cognitive functioning of patients with pre-existing dementia. *J. Alzheimers Dis. Rep.* **7**, 119–128 (2023).
37. Zhao, J., Xia, F., Jiao, X. & Lyu, X. Long COVID and its association with neurodegenerative diseases: pathogenesis, neuroimaging, and treatment. *Front. Neurol.* https://doi.org/10.3389/fneur.2024.1367974 (2024).
38. Karki, R. et al. Synergism of TNF-α and IFN-γ triggers inflammatory cell death, tissue damage, and mortality in SARS-CoV-2 infection and cytokine shock syndromes. *Cell* **184**, 149–168.e117 (2021).
39. Santos, J. G.dO. et al. Impact of SARS-CoV-2 on saliva: TNF-α, IL-6, IL-10, lactoferrin, lysozyme, IgG, IgA, and IgM. *J. Oral. Biosci.* **64**, 108–113 (2022).
40. Zhuang, Z. et al. Mapping and role of T cell response in SARS-CoV-2–infected mice. *J. Exp. Med.* **218**, e20202187 (2021).
41. Gu, T. et al. Cytokine signature induced by SARS-CoV-2 spike protein in a mouse model. *Front. Immunol.* https://doi.org/10.3389/fimmu.2020.621441 (2021).
42. Krishna, V. D. et al. Impact of age and sex on neuroinflammation following SARS-CoV-2 infection in a murine model. *Front. Microbiol.* https://doi.org/10.3389/fmicb.2024.1404312 (2024).
43. Torres, E. et al. Apolipoprotein E Isoform-specific changes related to stress and trauma exposure. *Transl. Psychiatry* **12**, 125 (2022).
44. Chornyy, S. et al. Longitudinal in vivo monitoring of axonal degeneration after brain injury. *Cell Rep. Methods* **3**, 100481 (2023).
45. Das, A. et al. Enhanced detection sensitivity of neuronal activity patterns using CaMPARI1 vs. CaMPARI2. *Front. Neurosci.* **16**, 1055554 (2023).
46. Das, A. et al. Large-scale recording of neuronal activity in freely-moving mice at cellular resolution. *Nat. Commun.* **14**, 6399 (2023).

47. Tennant, K. A. et al. The organization of the forelimb representation of the C57BL/6 mouse motor cortex as defined by intracortical microstimulation and cytoarchitecture. *Cereb. Cortex* **21**, 865–876 (2011).
48. Dana, H. et al. High-performance calcium sensors for imaging activity in neuronal populations and microcompartments. *Nat. Methods* **16**, 649–657 (2019).
49. Chen, T.-W. et al. Ultrasensitive fluorescent proteins for imaging neuronal activity. *Nature* **499**, 295–300 (2013).
50. Chornyy, S. et al. Cellular-resolution monitoring of ischemic stroke pathologies in the rat cortex. *Biomed. Opt. Express* **12**, 4901–4919 (2021).
51. Das, A. et al. Reversible loss of hippocampal function in a mouse model of demyelination/remyelination. *Front. Cell. Neurosci.* **13**, 588 (2020).
52. Thevenaz, P., Ruttimann, U. E. & Unser, M. A pyramid approach to subpixel registration based on intensity. *IEEE Trans. Image Process* **7**, 27–41 (1998).
53. Stringer, C., Wang, T., Michaelos, M. & Pachitariu, M. Cellpose: a generalist algorithm for cellular segmentation. *Nat. Methods* **18**, 100–106 (2021).
54. Kerlin, A. M., Andermann, M. L., Berezovskii, V. K. & Reid, R. C. Broadly tuned response properties of diverse inhibitory neuron subtypes in mouse visual cortex. *Neuron* **67**, 858–871 (2010).
55. Deneux, T. et al. Accurate spike estimation from noisy calcium signals for ultrafast three-dimensional imaging of large neuronal populations in vivo. *Nat. Commun.* **7**, 12190 (2016).
56. Das, A., Icardi, J., Borovicka, J. & Dana, H. Data and code for the publication: "Exposure to COVID-19 virus-like particles modulates firing patterns of cortical neurons in the mouse brain". *Figshare* https://doi.org/10.6084/m9.figshare.29238128 (2025).

Acknowledgements

The authors would like to thank Dr. Christopher Nelson for helpful comments and suggestions to improve the manuscript. The authors would like to thank the HHMI Janelia GENIE team for sharing the jGCaMP7s indicator, Dr. Vanzetta and their team for sharing the SpikeML algorithm, and Dr. Pachitariu and their team for sharing the CellPose software. This work was supported by grants R21AG065914 and R21AG065914-01S1 from the NIH/NIA.

Author contributions

H.D. and J.R. designed the study, A.J.H. designed the VLPs and H.F.H. produced them, A.D. and S.H. performed the experiments. J.I., J.B., and S.H. performed the data analysis. J.I. and J.R. performed the statistical analysis. H.D. and J.R. wrote the manuscript with comments from J.I. and A.J.H.

Competing interests

The authors declare no competing interests.

Additional information

Supplementary information The online version contains supplementary material available at https://doi.org/10.1038/s42003-025-08435-8.

Correspondence and requests for materials should be addressed to Hod Dana.

Peer review information *Communications Biology* thanks Fernando Peña Ortega and the other, anonymous, reviewer for their contribution to the peer review of this work.